

Article www.acsanm.org

# Au Nanoparticle/WS<sub>2</sub> Nanodome/Graphene van der Waals Heterostructure Substrates for Surface-Enhanced Raman Spectroscopy

Samar Ali Ghopry,\* Mohammed Alamri, Ryan Goul, Brent Cook, Seyed M. Sadeghi, Rithvik R. Gutha, Ridwan Sakidja, and Judy Z. Wu\*

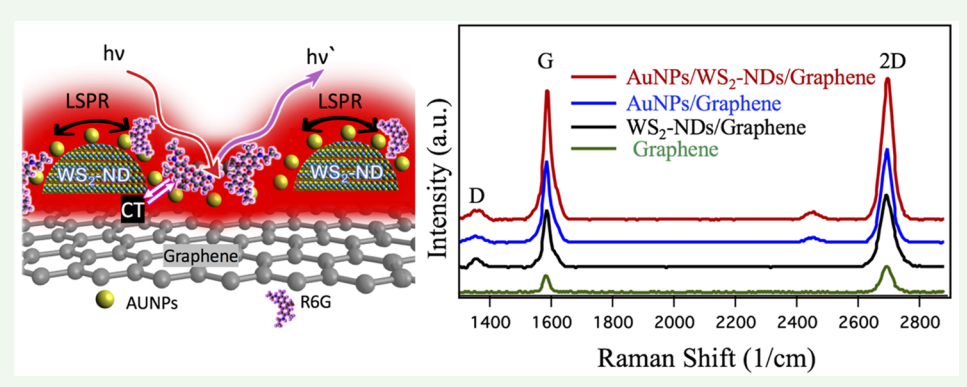


**ACCESS** 

Metrics & More

Article Recommendations

Supporting Information



ABSTRACT: This work explores superposition of the localized surface plasmonic resonance (LSPR) effect of Au nanoparticles (AuNPs) with that on transition metal dichalcogenide (TMD) WS<sub>2</sub> nanodomes (WS<sub>2</sub>-NDs) enabled by enhanced dipole-dipole interaction at van der Waals (vdW) interfaces in AuNP/WS2-ND/graphene heterostructures for surface-enhanced Raman spectroscopy (SERS) with high-sensitivity, The confirmation of such a superposition is first demonstrated in the enhanced graphene Raman signatures, such as the G-peak intensity by approximately 7.8 fold on the AuNP/WS2-ND/graphene over that of reference graphene sample, in contrast to 4.0- and 5.3-fold, respectively, on AuNP/graphene and on WS2-ND/graphene. Furthermore, Raman spectra of probe molecules of fluorescent Rhodamine 6G (R6G) were hired to quantify the enhanced SERS on AuNP/WS<sub>2</sub>-ND/graphene SERS substrates. At the R6G concentration of  $5 \times 10^{-5}$  M, enhancement factors of ~2.0 and 2.4 based on the R6G 613 cm<sup>-1</sup> peak intensity are detected on the AuNP/WS<sub>2</sub>-ND/graphene with respect to that on WS<sub>2</sub>-ND/graphene and AuNP/ graphene, respectively. The benefit of the superposition of the LSPR effects from the WS2-NDs and AuNPs results in high SERS sensitivity up to  $1 \times 10^{-12}$  M on AuNP/WS<sub>2</sub>-ND/graphene, which is about an order of magnitude better than what's on WS<sub>2</sub>-ND/ graphene, and several orders of magnitude better than that on the AuNP/graphene and metal nanostructure/TMD (continuous layer) substrates. This result reveals the advantage of superposition of the LSPR effects from different nanostructures through design of vdW heterostructures. In addition, considering the AuNP/WS2-ND/graphene vdW heterostructures can be fabricated in the layer-by-layer growth developed in this work, the high-sensitivity SERS substrates are scalable and low cost for marketable devices in optoelectronics and biosensing.

**KEYWORDS:** plasmonic Au/WS<sub>2</sub>-ND/graphene nanostructure, surface-enhanced Raman scattering, biosensing, van der Waals heterostructure, electromagnetic mechanism effect

## 1. INTRODUCTION

Surface-enhanced Raman spectroscopy (SERS) provides a powerful approach for detecting chemicals and biomolecules with high sensitivity allowing the detection even of single-molecule sensitivity. 1-4 SERS relies on an electromagnetic mechanism (EM) that provides the major participation of the enhancement (with factors up to  $1 \times 10^8$ ) and chemical mechanism (CM) with the minor participation. 5-9 The EM relies on the evanescent enhancement of the electromagnetic field generated at or near the metal surface nanostructures

because of the collective oscillation of the electron on the surface causing by light illumination. 10 On metal nanostructures, this

Received: December 13, 2019 Accepted: February 18, 2020 Published: February 18, 2020



oscillation leads to localized surface plasmon resonance (LSPR) that critically improves the EM enhancement factors.<sup>11</sup>

The CM is induced via charge transfer at the interface between the SERS substrate and probe molecules or analyte, which can be efficient when the substrate's Fermi level positions in between the highest occupied molecular orbital (HOMO) and the lowest unoccupied molecular orbital (LUMO) of the analyte. Considering this, two-dimensional (2D) materials, <sup>12</sup> for example, graphene and transition metal dichalcogenides (TMDs), are particularly interesting for attachment of probe molecules with suitable electronic structures to induce the CM effect.<sup>13-16</sup> For instance, Ling et al. reported SERS CM enhancement factors of 2-17 on graphene using multiple probe molecules including R6G.<sup>14</sup> Differing from the semimetallic graphene, the TMDs are semiconductors with bandgaps typically in the visible spectrum, which means their CM enhancement factors may be sensitively affected by the band edge alignment at their interface with analyte. 17-22 It is wellknown that R6G, as a dye molecule, emits light of 532 nm determined by the bandgap energy in between its HOMO and LUMO energy levels.<sup>23,24</sup> This means the resonance Raman spectra of R6G at the 532 nm excitation would provide the best sensitivity as compared to that at nonresonance Raman excitations wavelengths. 23,24 Lee et al. investigated the resonant SERS enhancement of R6G (with a resonance wavelength ~532 nm) on 2D materials including graphene, MoS2, and WSe2 flakes.<sup>25</sup> The R6G SERS enhancement factors on MoS<sub>2</sub> and WSe<sub>2</sub> flakes were found to be about 0.5 and 1.7 times of that on exfoliated graphene, respectively. Using 532 nm excitation laser, Anbazhagan et al. also investigated resonant SERS enhancement of R6G on the lithium-exfoliated MoS<sub>2</sub> (Li-MoS<sub>2</sub>) and thioglycolic acid-exfoliated MoS<sub>2</sub> (T-MoS<sub>2</sub>).<sup>26</sup> They have found that the CM enhancement factor on the metallic phase of Li-MoS<sub>2</sub> is up to  $3.34 \times 10^3$  and  $1.7 \times 10^3$  for the 611 and 1647 cm<sup>-1</sup> R6G bands, respectively. Similarly, the CM enhancement factors of  $1.7 \times 10^3$  and  $5.6 \times 10^2$  for the same R6G bands were also observed on metallic T-MoS2. These results suggest that the semimetallic or doped 2D materials are favorable to achieve high SERS CM enhancement. On the Li-MoS<sub>2</sub> and T-MoS<sub>2</sub> substrates, the best resonant SERS sensitivity of R6G are  $1 \times 10^{-8}$  M and  $1 \times 10^{-7}$  M, respectively, <sup>27</sup> which are comparable to that obtained on graphene  $(5 \times 10^{-7} \,\mathrm{M})$ . More recently, heterostructures of two dimension materials have arisen as a favorable candidate for higher-sensitivity SERS substrates via electronic structure tuning at the van der Waals force (vdW) interfaces. As the CM effect depends on the interface electronic structures between the substrate and the analyte, tuning the electronic structure of the substrate is a key to enhancing the CM effect. 12,29-31 Using CuPc as a probe molecule, Tan et al. investigated the SERS CM enhancement factors on graphene/WSe2 vdW heterostructures, both produced via chemical vapor deposition (CVD), graphene, and WSe<sub>2</sub>, and observed a higher enhancement factor of 28.6 on the WSe<sub>2</sub>/graphene vdW heterostructure substrates, in contrast to 4.7 on graphene and 9.9 on WSe<sub>2</sub> only. 12

The SERS CM enhancement on 2D materials can be combined with the EM enhancement through implementation of plasmonic nanostructures on 2D materials. Goul et al. and Lu et al. have reported high sensitivity SERS substrate by integrating graphene with plasmonic Au nanoparticles (AuNPs) 22,36 using in situ metal evaporation at elevated temperatures for a clean metal/graphene interface and high SERS performance. Xu et al. have reported a reversed structure

by covering an AuNP array with graphene to enhance the molecular attachment area.  $^{38}$  High SERS sensitivity of R6G molecules up to  $1 \times 10^{-11}$  M was obtained in both cases hiring the 532 nm resonant excitation in wavelength. On the other hand, Chen et al. observed resonant SERS sensitivity of  $1 \times 10^{-9}$ M of R6G on an inverted MoS<sub>2</sub>/AgNPs SERS substrate by synthesizing a few sheets of MoS2 on top of AgNPs using thermal decomposition.<sup>39</sup> More recently, Shorie et al. synthesized AuNP/WS2 nanohybrids using liquid phase exfoliation of WS2 flakes, followed with in situ deposition of AuNPs. 40 Resonance SERS sensitivity of  $1 \times 10^{-8}$  M for R6G was obtained on this substrate. Besides single 2D materials. SERS enhancement of AuNP-decorated 2D (continuous layer) MoS<sub>2</sub>/graphene vdW heterostructures has also been explored.<sup>41</sup> The sensitivity of R6G up to  $5 \times 10^{-8}$  and  $5 \times 10^{-10}$  M was obtained on the substrate using excitation of 633 and 532 nm, respectively.

It should be pointed out that TMD nanostructures can also provide strong SERS EM enhancement. In a recent work, we fabricated TMD nanodome/graphene vdW heterostructures with the TMD nanodomes (TMD-NDs) including WS2-NDs and MoS<sub>2</sub>-NDs with a lateral dimension of 200-500 nm and vertical dimension of 3-5 nm decorated on monolayer CVD graphene sheet. A strong LSPR effect is enabled, leading to a remarkable resonant R6G SERS sensitivity of  $\sim 1 \times 10^{-11}$  M on the WS<sub>2</sub>-ND/graphene vdW heterostructures.<sup>28</sup> This sensitivity is comparable to the best reported on metal NP/2D material SERS substrates. In this work, the superposition of the LSPR effects of AuNPs and TMD-NDs of AuNP/WS2-ND/ graphene vdW heterostructures is further investigated. Remarkably, resonant SERS sensitivity of the R6G up to  $1 \times 10^{-12}$  M has been obtained on the AuNP/WS2-ND/graphene, which is one order of magnitude enhancement over the best reported on the TMD-ND/graphene and metal NP/graphene (or other 2D materials) SERS substrates.

#### 2. SIMULATION AND EXPERIMENTAL SECTION

Growth of CVD Graphene. Graphene samples were produced via a CVD system on polycrystalline copper sheets (Alfa Aesar) in a quartz pipe inner CVD furnace at 1050 °C with a combination of  $\rm H_2/CH_4$  with (7 sccm/40 sccm), followed with wet transfer on silicon substrate using a multistep process that was described previously. 42,43 In short, poly(methyl methacrylate) (PMMA) was spin-coated (3000 rpm) on graphene film and then the samples were annealed at 120 °C. Afterward, the Cu/graphene/PMMA samples were immersed (with the Cu side down) for about 4 h in copper etchant to completely remove the Cu foil. The suspended graphene/PMMA layer was then moved to deionized water multiple times to rinse the residual copper etchant. The graphene/PMMA sheets were moved onto the SiO<sub>2</sub> (90 nm)/Si. The graphene/PMMA films were left to drying over the night. The PMMA coating was removed via soaking in acetone (approximately five times) and isopropanol (IPA), then dried with N<sub>2</sub> gas gun. The samples were annealed at 400 °C in a mix of Ar/H<sub>2</sub> gas (500 sccm/300 sccm) for 30 min to clean the polymer residues on the graphene samples.

WS<sub>2</sub>–ND Synthesis on Graphene. The ammonium tetrathiotungstate (NH4)<sub>2</sub>WS<sub>4</sub> precursor solution (concentration of 0.1 wt %) was made by dissolving into (N, N-dimethylformamide, DMF). The transferred graphene samples were then immersed into the solution, followed by spin-coating at 3000 rpm for 1 min to obtain an ultrathin uniform film that can be segregated and formed into nanodomes on top of graphene with heating. <sup>28</sup> The samples were then thermally annealed at about 450 °C for ~30 min in the quartz tube of a CVD furnace with a mixed gas of  $H_2$  (10 sccm) and Ar (50 sccm). The powder of sulfur was located inside a quartz tube at the upstream zone of at a distance of ~25 cm from the sample and the sulfur source temperature was approximately at 200 °C.

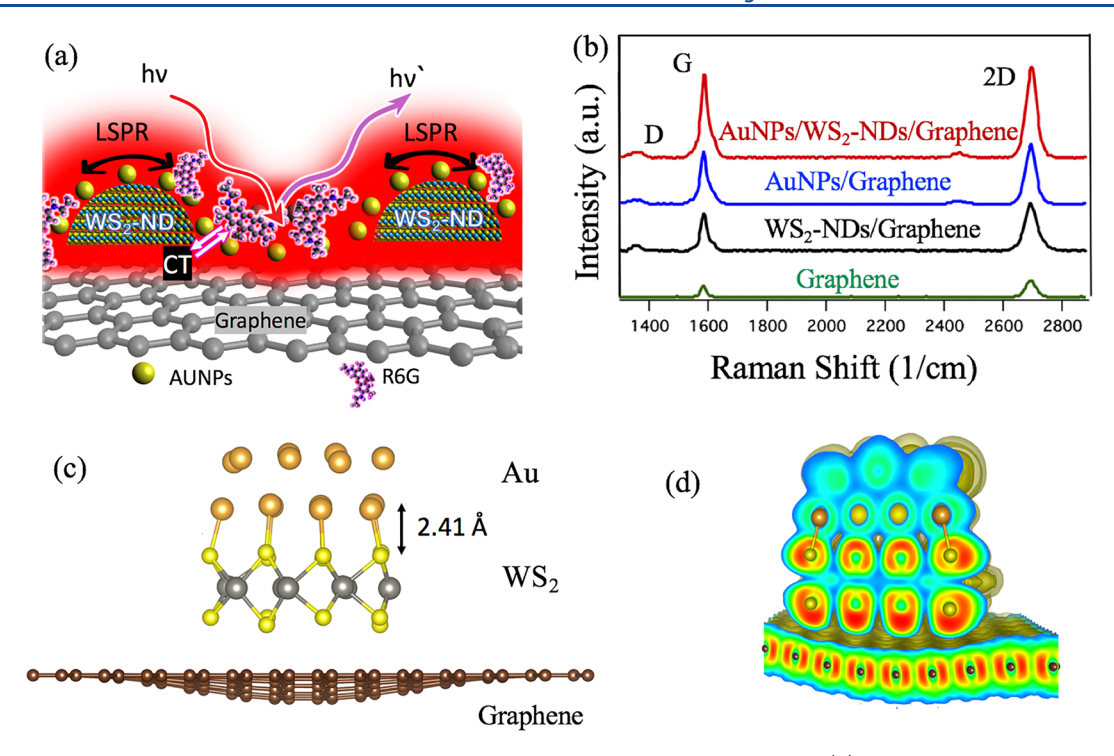


Figure 1. (a) Schematic design of the AuNP/WS $_2$ -ND/graphene vdW heterostructure SERS substrate. (b) Raman spectra of graphene taken on four samples: graphene only (green), WS $_2$ -ND/graphene (black), AuNP/graphene (blue) and AuNP/WS $_2$ -ND/graphene (red) using 488 nm laser of power of 1 mW. (c) Schematic illustration of the atomic layer stack of Au/WS $_2$ /graphene hybrid heterostructures with the interface distance between the AuNPs and WS $_2$  labeled. (d) 3D ELF plot of the stack of Au/WS $_2$ /graphene heterostructure shown in Figure 1c.

Fabrication of Plasmonic AuNPs on WS<sub>2</sub>–ND/Graphene. Plasmonic AuNPs were formed in a high vacuum via heat-assisted self-assembly during e-beam evaporation of Au of nominal thickness of 10–12 nm with the evaporation time of  $\sim\!90$  s (growth rate of 0.11–0.13 nm/s) on the WS<sub>2</sub>/graphene heterostructure samples at the sample temperature  $\sim\!300$  °C using a similar process we have developed for fabrication plasmonic metal NPs of Au and Ag on graphene and other 2D materials for optimal SERS effects.  $^{32,41,44}$  The reference samples of AuNP/graphene were fabricated using the same condition.

Characterization of AuNP/WS<sub>2</sub>–ND/Graphene SERS Substrates. Surface morphology, crystallinity, and microstructure of the WS<sub>2</sub>–ND/graphene heterostructures were examined using scanning electron microscopy (SEM)/energy-dispersive X-ray spectroscopy (EDS), atomic force microscopy (AFM), and Raman spectroscopy employing a WiTec alpha 300 confocal Raman system with laser excitation of 433 nm.

Raman Spectra of R6G on AuNP/WS2-ND/Graphene and AuNP/Graphene SERS Substrates. For SERS characterization of R6G probe molecules, a R6G droplet (with diameter of 4-5 mm and concentration from  $5 \times 10^{-5} \,\mathrm{M}$  to  $10^{-12} \,\mathrm{M}$ ) was casted onto the surface of the substrates and placed on a hot plate for 1 h (at 70  $^{\circ}\text{C})$  for drying the solvent. Raman spectroscopy with laser excitation of 532 nm, via a WiTec alpha 300 confocal Raman system, was used for SERS characterization. The molecules areal density can be roughly calculated from the R6G concentration, the volume of the droplets, and the dimension of the R6G samples on the SERS substrates. For a droplet of  $\sim$ 4-5 mm in diameter and R6G concentration of 5 × 10<sup>-5</sup> M, the R6G molecules number in the droplet is around 1012 molecules. After the R6G droplet dried, a circular spot with area of ~12 mm<sup>2</sup> was formed. The number of molecules per unit area in the spot can be estimated via dividing the calculated R6G molecules number in the drop by the dried spot area. Thus, the number of molecules per unit area in the spot  $\sim$ 1  $\times$  $10^4$  to  $1 \times 10^5$  molecules/ $\mu$ m<sup>2</sup> at dilution of the  $5 \times 10^{-5}$  M and  $\sim 2 \times 10^{-5}$  M  $10^{-2}$  molecules/ $\mu$ m<sup>2</sup> at dilution of the 5 ×  $10^{-12}$  M. With the laser beam area, the number of molecules under detection can be estimated. The submillimeter laser beam spot (approximately tens of micrometers in dimeter) with a 20× microscope objective was sensibly small letting

multiple scan positions in the center of every droplet during the R6G Raman measurement. A small integration time of 3 s and a low intensity ( $\sim 1-5$  mW) were applied to prevent the possible damage of the R6G molecules. In order to improve the signal-to-noise ratio, every individual demonstrated spectrum is an average of multiple spectra collected at the same spot of the sample. It should be noticed that each Raman spectra presented in this work are representative based on average of multiple (typically 6–10) Raman spectra collected at spots randomly selected on a sample to demonstrate reproducibility and consistency. The spots were selected not too close to the droplet's edge of the sample to avoid the coffee-ring effect. Figures S1a, b illustrates nine such spectra taken on a sample with 5 × 10<sup>-5</sup> M R6G molecules and the histogram of the 613 cm<sup>-1</sup> peak intensity of the nine spectra, respectively.

Density Function Theory (DFT) and Finite-Difference Time-Domain (FDTD) Simulation. The DFT<sup>45</sup> method was employed to compute the electronic structure of AuNP/TMD<sub>2</sub>/graphene 2D vdW heterostructure as obtained in Vienna ab initio simulation package (VASP). 46 These hybrid systems involve a combination of TMDs sheet of MoS<sub>2</sub> (WS<sub>2</sub>) and one to multilayers of Au (111) with varied thicknesses as detailed in our previous publication.<sup>41</sup> It is important to note that a thicker Au layer (2 monolayers or 2L, and multilayers) was found to lead to reduction of the interatomic distance because of enhanced dipole-dipole interaction and electron delocalization of TMD-NDs at the Au/TMD interface, which promote the plasmonic EM effect. 41 For the FDTD simulation, the focus was to highlight the impact of the plasmonic AuNPs on the AuNP/TMD-ND/graphene heterostructures. Specifically, we numerically studied the interaction of light with an Au semispherical NP (with a 40 nm diameter) placed on a layered structure consisting of a SiO<sub>2</sub> substrate covered with 5 nm of a high refractive index (n = 4.4) dielectric material regarding multiple The simulation was done using the Lumerical published works.<sup>47-</sup> FDTD solutions software, considering a plane wave reaching the AuNPs from the top along the *z*-axis. For the 5 nm dielectric materials, we used Ge from the library of this software. In terms of refractive index, for the range of wavelengths considered here, i.e., ~550 nm, Ge is similar to WS2. They have, however, different absorption, which can

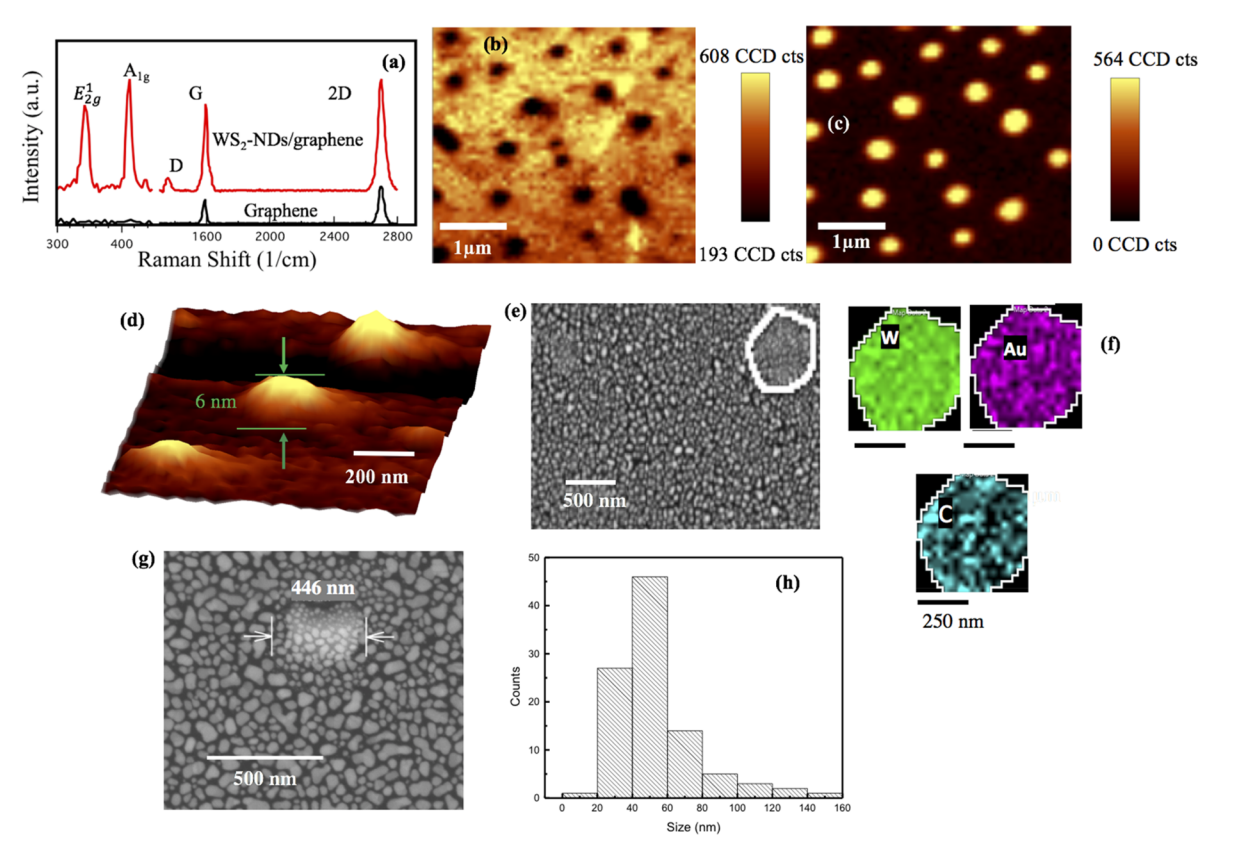


Figure 2. (a) Raman spectrum of WS<sub>2</sub>–ND/graphene vdW heterostructure and graphene. (b, c) Raman map of graphene (2D mode) and WS<sub>2</sub> ( $E_{2g}^{1}$  mode) on graphene, employing the 488 nm excitation laser. (d) Representative AFM image of the WS<sub>2</sub>–NDs; (e, f) SEM image of an AuNP/WS<sub>2</sub>–ND/graphene sample and EDS maps of W (green), Au (purple) and C (blue). (g) A zoom-in SEM image of the same sample and (h) a particle size distribution histogram taken on the selected area marked in g.

influence the extinction spectrum. As the thickness of the dielectric is very small, we do expect this significantly changes the wavelengths of the plasmonic modes and their near fields.

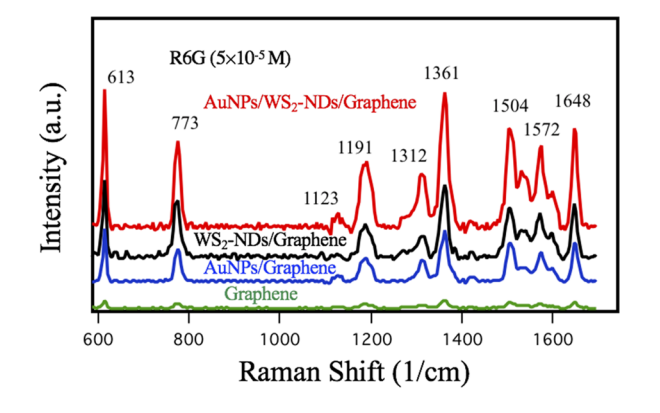
## 3. RESULTS AND DISCUSSION

Figure 1a schematically demonstrates the SERS substrate of AuNPs/WS<sub>2</sub>-ND/graphene vdW heterostructure for R6G detection. The Raman signatures of the R6G probe molecules attached to the substrate are expected to be enhanced due to both the EM and CM effects. For quantify the LSPR enhancement by the integrated plasmonic AuNP/WS2-NDs, graphene Raman spectra were taken on graphene only, WS2-ND/graphene, and AuNP/WS<sub>2</sub>-ND/graphene and the results are depicted in Figure 1b. On all four samples, the graphene's defect D-peak at ~1356 cm<sup>-1</sup> has an insignificant intensity, confirming the high quality of the graphene synthesized using CVD for this work. The two main signatures of graphene, i.e., the G peak at ~1587 cm<sup>-1</sup> due to a primary in-plane displacement  $(E_{2g})$  mode and the 2D peak at 2695 cm<sup>-1</sup> due to a secondary inplane displacement of zone-boundary phonons, are clearly observable in Figure 1b. On the graphene-only sample (green), the ratio of the graphene peak intensities (2D over G) is around 2.1, which is expected for monolayer graphene. However, the peak intensities differ quantitatively because of the LSPR effect at the same Raman measurement condition of 488 nm excitation of 1 mW power. In fact, the intensities of the graphene peaks (both G and 2D) are considerably boosted with decoration of the plasmonic WS<sub>2</sub>-NDs (black), plasmonic AuNPs (blue), and AuNP/WS<sub>2</sub>-NDs (red). On the samples of WS<sub>2</sub>-ND/ graphene and AuNP/graphene, the enhancement factors of the

graphene G peak and 2D peaks are, respectively, 4.0 and 3.0 and 5.3 and 4.0, which are comparable to that reported previously on plasmonic metal nanostructures/graphene. <sup>32,50,51</sup> On the AuNP/WS<sub>2</sub>-ND/graphene substrate, the enhancement factors of the graphene G and 2D peaks is further increased to about 7.8 and 5.6, respectively, which may be attributed to the superposition of the LSPR effects of AuNPs and WS<sub>2</sub>-NDs in the AuNP/WS<sub>2</sub>-ND/graphene vdW heterostructures. The enhancement of the LSPR effect of the AuNP/WS2-NDs is most probably caused by the increased dipole-dipole interaction at the AuNP/WS<sub>2</sub>-ND/graphene vdW interface as shown in a density function theory simulation (DFT).<sup>41</sup> Figure 1c demonstrates the Au/WS<sub>2</sub>/graphene heterostructures side view of two atomic layers of Au after process of the relaxation in DFT simulation. The electronic structure of the interface between MoS<sub>2</sub> (or WS<sub>2</sub>) 2D layer and 1-6 atomic layers of Au was reported recently. 41 It has been found that varying the layer number of the Au from monolayer (1L) to a few layers can lead to a significant reduction of the interatomic spacing at the Au/MoS<sub>2</sub> interface, which consequently results in charge transfer enhancement in the AuNP/MoS<sub>2</sub>/graphene hybrid system. Specifically, the interatomic distance is around 3.03 Å in the case of Au (1L) on top on  $MoS_2$ , and it reduces about 20% to around 2.47 Å when the Au layer number is increased to two layers (2L) or more. On Au (2L)/WS<sub>2</sub>(1L)/ graphene, the interatomic distance is around 2.41 Å as shown in Figure 1c. An enhanced charge transfer is therefore anticipated because of the improvement in the dipole—dipole interaction at a reduced interatomic distance, resulting in enhanced SERS on Au (2L) or multilayer on WS<sub>2</sub>/graphene heterostructures. In addition, 3D plans of the electron localization function (ELF) were investigated and delocalized electron level was shown to be limited on a monolayer of Au/MoS<sub>2</sub>. <sup>41</sup> In contrast, delocalized electron level increases in the attendance of 2L Au layers or thicker. Figure 1d demonstrates the 3D plot of the ELF in the 3L-Au/WS<sub>2</sub>/graphene heterostructures. It can be seen that the ELF has a normalized scale of 0–1 with greater values (more red) revealing improvement of the localized electrons in "C-form" red contour configurations attaching S atoms to W atoms.

The Raman spectra taken on graphene and on the vdW heterostructure of WS<sub>2</sub>-ND/graphene is shown in Figure 2a. Besides the graphene signature peaks at ~1587 cm<sup>-1</sup> (for G band) and ~2695 cm<sup>-1</sup> (for 2D band) and a minor disorder produced (D band) at ~1350 cm<sup>-1</sup>, the Raman peaks associated with the WS<sub>2</sub>-NDs created on graphene monolayer can be seen at  $\sim$ 342 cm<sup>-1</sup> (E<sub>2g</sub><sup>1</sup>) and  $\sim$ 412 cm<sup>-1</sup> (A<sub>1g</sub>) due to, respectively, the S and Mo atoms in-plane vibration and the S atoms out-ofplane vibration. 52 Figure 2b, c shows the graphene (2D mode) Raman maps and  $WS_2$  ( $E_{2g}^1$  mode) on the sample of  $WS_2$ -NDs/graphene using the 488 nm excitation laser in wavelength. The graphene's Raman map shows continues distribution with lower intensity on the location covered by the WS2-NDs. The WS2 (E<sub>2g</sub> mode) Raman map exhibits an opposite intensity distribution, demonstrating the formation of the WS2-NDs with lateral dimension on the order of 300-500 nm. Figure 2d displays the WS<sub>2</sub> nanodomes AFM image, with the lateral dimension of 300-500 nm and height around 4-6 nm have been identified for the nanodomes. Figure 2e, f displays the SEM images and EDS maps of W (in green), Au (in purple), and C (in blue), respectively, of an AuNP/WS<sub>2</sub>/graphene heterostructures. The W, Au, and C elemental mapping analyses confirm the uniform distribution of the AuNPs and WS<sub>2</sub>-NDs on top of graphene with the lateral dimension consistent to that shown in AFM analysis and Raman map. The zoom-in SEM image of the same sample shown in Figures 2g and the particle size distribution histogram (Figures 2h) on the selected area marked on the SEM image show that the AuNPs are decorated uniformly throughout the sample including on top of the WS<sub>2</sub>-NDs. Most AuNPs have approximately round shapes of lateral dimension in the range of  $\sim$ 40–50 nm. Under the nominal Au thickness of 10-12 nm, the height of the AuNPs is in the range of 10-15 nm.<sup>32</sup>

Figure 3 demonstrates the comparison of R6G (with a concentration of  $5 \times 10^{-5}$  M) Raman spectra on AuNPs/WS<sub>2</sub>–



**Figure 3.** Raman spectra of R6G molecules at the concentration of  $5 \times 10^{-5}$  M deposited on AuNP/WS<sub>2</sub>–ND/graphene (red), WS<sub>2</sub>–ND/graphene heterostructure substrates (black) and AuNP/graphene (blue) with excitation length of 532 nm.

ND/graphene heterostructures (red), WS2-ND/graphene heterostructures (black), AuNP/graphene (blue) and graphene (green) substrates hiring the same excitation length of 532 nm. Series peaks of R6G Raman signature can be recognized on all three spectra including the 613 cm<sup>-1</sup> peak assigned to in-plane vibration mode of C-C-C ring, 769 cm<sup>-1</sup> peak assigned to aromatic bending mode of C-H, and the 1312 and 1502 cm<sup>-1</sup> peaks assigned to in plane bend mode of N-H. The peaks at 1361, 1504, 1576, and 1648 cm<sup>-1</sup> can be assigned to the stretching mode of C-C and the 1190 cm<sup>-1</sup> peak can be assigned to the stretching mode of C-O-C, respectively. 13,53,54 For R6G on graphene substrate, the spectrum shows visually low Raman signature intensity as compared to the spectra on the other three substrates in the same figure. By using the R6G feature peak at 613 cm<sup>-1</sup> on graphene as the reference, the enhancement factors of 10.3 and 8.7 have been obtained on WS2-ND/graphene and AuNP/graphene substrates, respectively. Furthermore, the enhancement factor is increased to 21.2 on the AuNP/WS<sub>2</sub>-ND/graphene heterostructures, indicating the benefit of superposition of the SERS enhancements by plasmonic AuNPs and WS2-NDs. Interestingly, the R6G Raman signatures have comparable intensities on the WS<sub>2</sub>-ND/graphene and AuNP/graphene substrates, suggesting the SERS enhancement factors by the plasmonic AuNPs and WS<sub>2</sub>-NDs are comparable. This is not surprising considering both AuNPs and TMD–NDs (WS<sub>2</sub>–ND<sub>S</sub> and WS<sub>2</sub>–ND<sub>S</sub>) are strong plasmonic nanostructures because of the EM effect.<sup>28,32,3</sup> However, the R6G Raman signatures are considerably enhanced on the AuNP/WS<sub>2</sub>-ND/graphene heterostructures comparing to that on the WS2-ND/graphene and AuNP/graphene substrates. For example, the 613 cm<sup>-1</sup> R6G peak is a factor of 2.0 and 2.4 stronger on the AuNP/WS2-ND/graphene substrate than on the WS<sub>2</sub>-ND/graphene and AuNP/graphene substrates, respectively. Similarly, the enhancement factors of the R6G signature at 773 cm<sup>-1</sup> are 1.6 and 2.4, respectively. This observed SERS enhancement illustrates the benefit of the superposition of the LSPR effects from the WS2-NDs and AuNPs in the AuNP/WS2-ND/graphene vdW heterostruc-

For probing the SERS sensitivity on the AuNP/WS<sub>2</sub>-ND/ graphene vdW heterostructure substrates, R6G molecules Raman spectra of different concentrations as low as  $1 \times 10^{-12}$ M were collected employing the R6G resonance excitation length of 532 nm. For a comparison, the same experiment was repeated on the WS2-ND/graphene and AuNP/graphene substrates and the results are shown in Figure 4a-c. On the substrate of AuNP/WS2-ND/graphene vdW heterostructure, all Raman signatures of R6G are visible at higher R6G concentrations above  $5 \times 10^{-12}$  M. With further reduction of the R6G concentration, the R6G visible signature modes are reduced to a few vibrational modes, such as 613, 773, and 1191 cm<sup>-1</sup>, with greater polarizability. In fact, the 613 cm<sup>-1</sup> peak remains detectable at the lowest R6G concentration of  $1 \times 10^{-12}$ M. For a comparison, the R6G Raman spectra on both WS<sub>2</sub>-ND<sub>S</sub>/graphene and AuNPs/graphene substrates are shown in Figures 4b, c. The Raman signatures of R6G are visible up to the lowest R6G concentrations of  $5 \times 10^{-11}$  M on WS<sub>2</sub>-ND/ graphene and  $5 \times 10^{-9}$  M on AuNP/graphene substrates. This indicates that the R6G SERS sensitivity is indeed enhanced through superposition of the LSPR effects of AuNP and WS<sub>2</sub>-NDs on the AuNP/WS<sub>2</sub>/graphene vdW heterostructure substrates. In addition, the resonant Raman spectra (with 532 nm Raman excitation) of the R6G on AuNP/WS<sub>2</sub>-NDs were

**ACS Applied Nano Materials** 

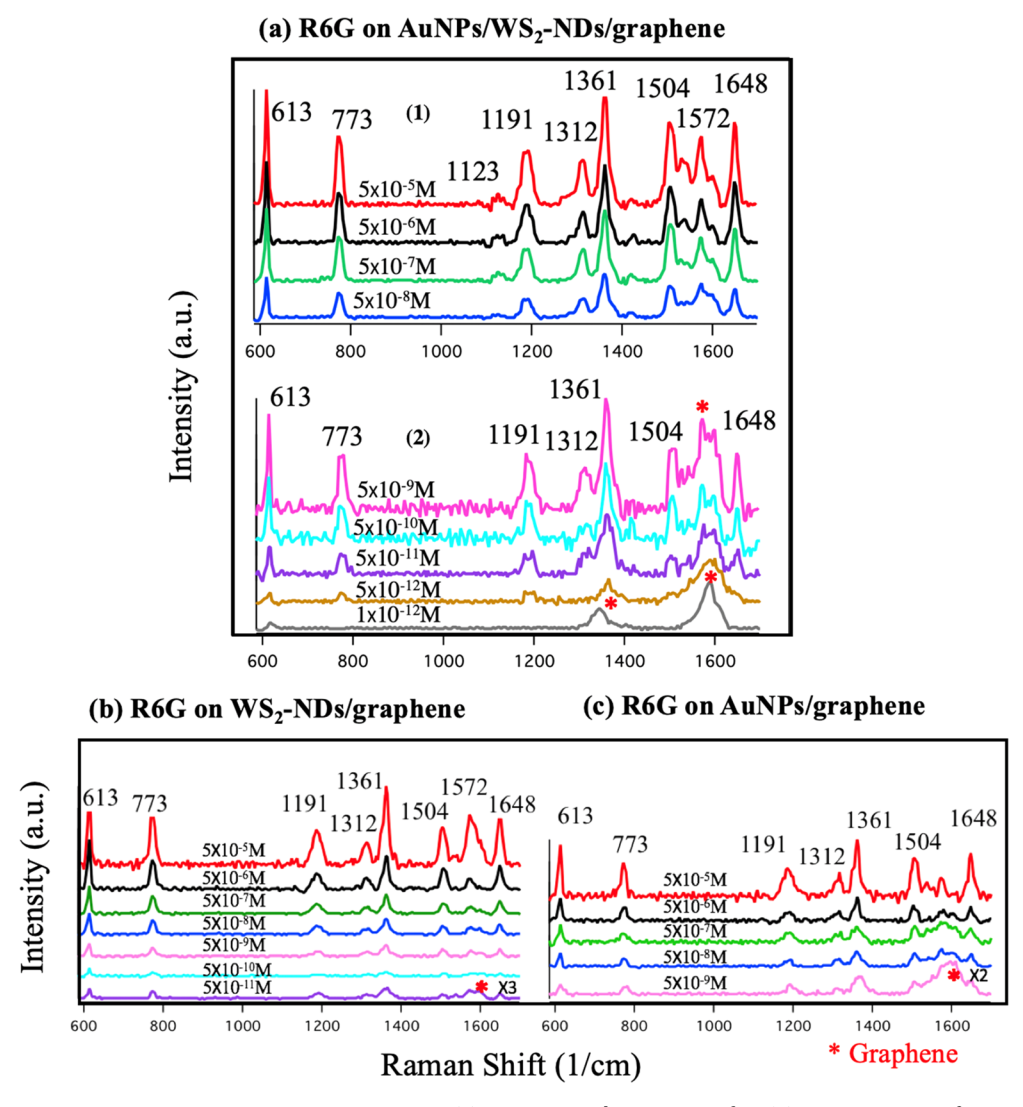


Figure 4. R6G molecules Raman spectra with varied concentrations (a) from  $5 \times 10^{-8}$  M to  $5 \times 10^{-8}$  M (1) and from  $5 \times 10^{-9}$  M to  $1 \times 10^{-12}$  M (2) on the AuNP/WS<sub>2</sub>–ND/graphene with excitation of 532 nm laser; R6G molecules Raman spectra with varied concentrations: (b) from  $5 \times 10^{-5}$  M to  $5 \times 10^{-11}$  on the WS<sub>2</sub>–ND/graphene (the spectrum of the concentration  $5 \times 10^{-11}$  M was multiplied by 3 for better visibility); and (c) from  $5 \times 10^{-5}$  M to  $5 \times 10^{-9}$  on the AuNP/graphene substrates (the spectrum of the concentration  $5 \times 10^{-9}$  M was multiplied by 2 for better visibility). All spectra were taken with 532 nm excitation laser of the same power.

taken as shown in Figure S2. The lower sensitivity of about 5 ×  $10^{-10}$  M is about one order of magnitude better than that of 5  $\times$ 10<sup>-9</sup> M on the AuNP/TMD continuous layer substrates, <sup>41</sup> which can be attributed to the EM effect enabled in the TMD-NDs. Overall, the AuNP/WS2-ND/graphene heterostructure substrate shows the best SERS enhancement, which is higher than that on AuNP/graphene or WS<sub>2</sub> only, and to AuNP/WS<sub>2</sub>, implying the EM enhancement through superposition of the SERS from plasmonic AuNPs and WS2-NDs enhanced by the interfaces in the AuNP/WS2-ND/graphene heterostructures and the CM enhancement of graphene. 28,41 In fact, the higher SERS sensitivity of the AuNP/WS<sub>2</sub>/graphene is more than an order of magnitude improvement over that of the WS<sub>2</sub>-ND/ graphene and about three orders of magnitude better than that of AuNPs/graphene.<sup>28</sup> To the best of our knowledge, the R6G sensitivity of  $1 \times 10^{-12}$  M of the AuNP/WS<sub>2</sub>/graphene is one order of magnitude better than the best resonance R6G sensitivity so far reported using the plasmonic metal nanostructure/graphene substrates, 38 and by about one to four orders of magnitude better than that on the TMDs

(continuous strates. layer)/metal nanostructure SERS substrates. In fact, the further enhanced R6G SERS sensitivity illustrated in Figure 4 is consistent with the enhanced graphene signature enhancement shown in Figure 1 on AuNP/WS<sub>2</sub>/graphene, which can be attributed to the superposition of the LSPR effects from AuNPs and WS<sub>2</sub>–NDs in the AuNP/WS<sub>2</sub>–ND/graphene heterostructures.

Figure 5a-d illustrates the R6G Raman peak intensities at 613 and 773 cm<sup>-1</sup>, respecitively, as a function of the R6G concentration on AuNPs/WS<sub>2</sub>-ND/graphene vdW heterostructures. Figure 5a, c displays the logarithmic correlation between the peak intensity of R6G Raman spactra and R6G concentration using linear scale for the R6G concentration axis with the fitting equation of  $y = \log x + m$ , whereas Figure 5b, d shows the same plots on a logarithmic scale for the R6G concentration axis. An approximately logarithmic relation can be observed since the fitting equation of  $y = \log x + m$  well fits the SERS intensity vs concentration curves as shown in Figure 5a, c, which is expected from the superposition of the plasmonic enhancement of the AuNPs and WS<sub>2</sub>-NDs. Indeed, this

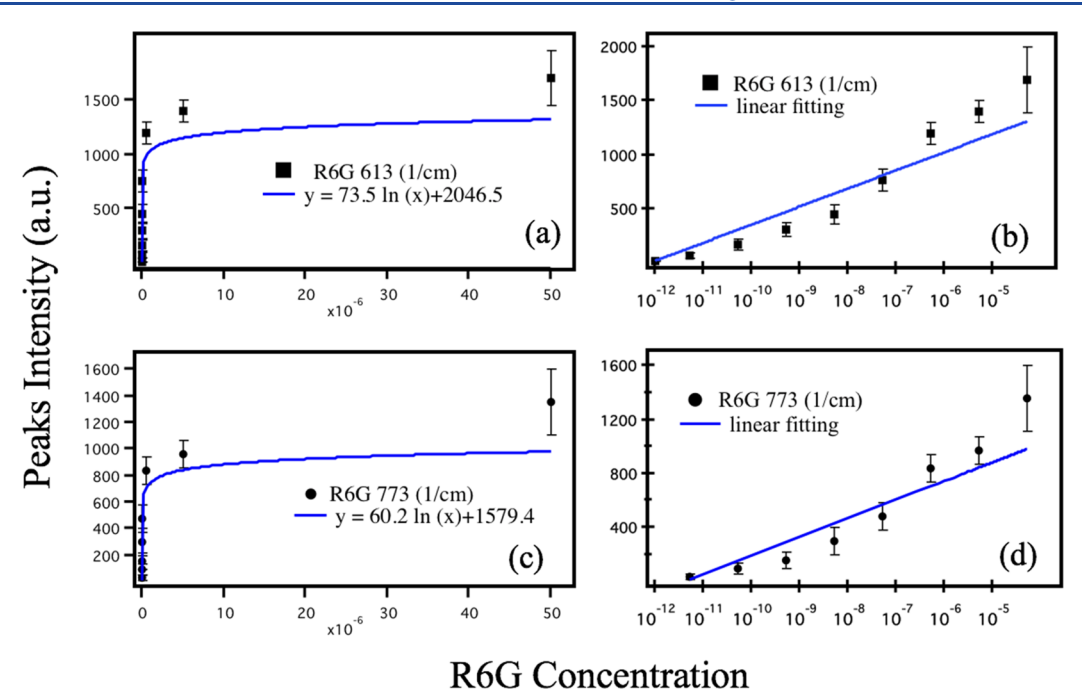
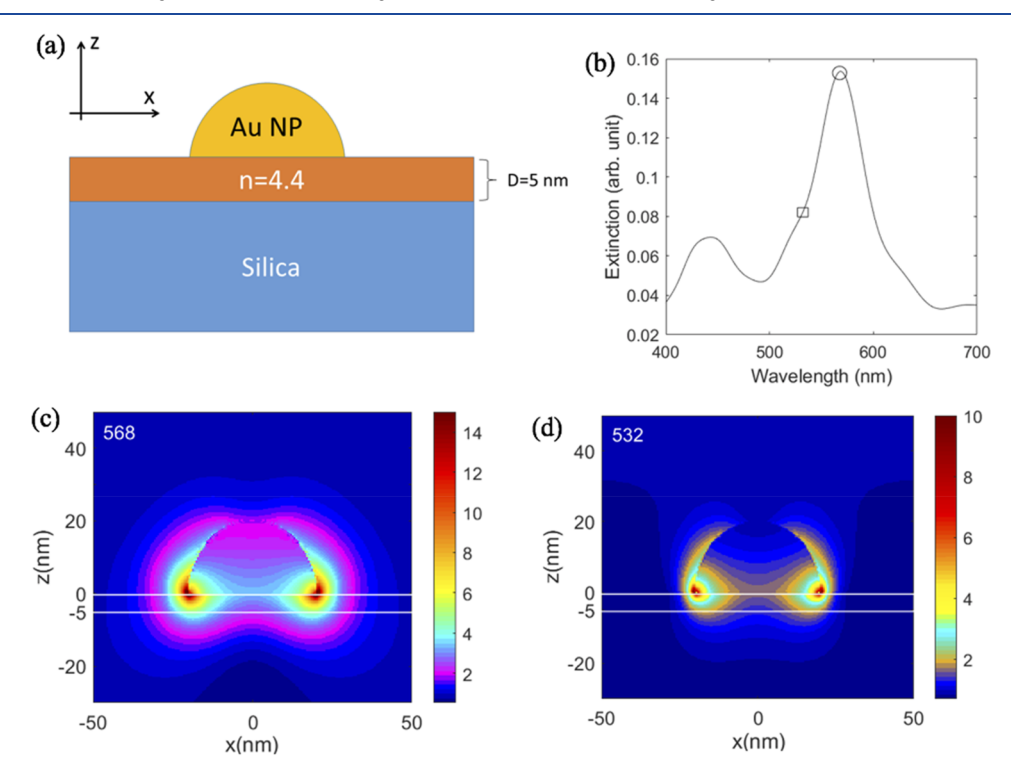


Figure 5. (a-d) Relation between the intensities of the Raman peaks and the R6G concentrations at (a, b) 613 and (c, d) 773 cm<sup>-1</sup> for the AuNP/WS<sub>2</sub>-ND/graphene substrate using 532 nm laser and using (a, c) a linear scale and (b, d) a logarithmic scale.



**Figure 6.** (a) Diagram of the structure adopted for simulations of plasmonic response of the Au NP. (b) Simulated extinction spectrum of the structure. The circle and square refer here to the wavelengths of the peak and incident laser used for SERS, respectively. (c, d) Simulated plasmonic modes of the Au NP at 568 and 532 nm. The scale bars are color-coded presentation of  $P_{enh}$  around the NP.

logarithmic relation between the SERS intensity and concentration is noted in earlier reports of SERS sensitivity using analyte molecules with various kinds. <sup>15,36,56,57</sup> However, the few higher R6G concentration data points does not look to fit the trends as well as the lower R6G concentration data points, which was also observed in our previous report of MoS<sub>2</sub> (WS<sub>2</sub>)–ND/graphene vdW heterostructures SERS sensitivity using R6G. <sup>28</sup>

Considering SERS sensitivity is primarily determined by the EM effect, understanding the mechanism of the superposition of the evanescent electromagnetic fields by the AuNPs and  $WS_2$ –NDs is important. Depending on the shapes and sizes of metallic NPs and the materials they made of, plasmonic EM enhancement can, in general, increase the effective intensity of the incident light and shorten radiative decay lifetimes of molecules

(Purcell effect). The plasmonic properties of the WS<sub>2</sub>–NDs studied in this paper are partially associated with their optical doping. As a result, a primary impact of AuNPs can be enhancement of excitation rates of such WS<sub>2</sub>–NDs via plasmonic effects, i.e.,  $I_{\rm eff} = P_{\rm enh}I_0$ , wherein  $P_{\rm enh}$  refers to the plasmon field enhancement factor, described as the ratio of the squares of the field in the presence of AuNPs to that when the AuNP is absent, and  $I_0$  represents the incident light intensity.

Figure 6a illustrates schematically the structure for the finitedifference time-domain (FDTD) simulation. Specifically, the structure includes a semispherical AuNP of 40 nm in diameter on top of a layered structure consisting of a SiO2 substrate covered with 5 nm thick TMD that is treated as a high refractive index dielectric material. Figure 6b shows the extinction spectrum of such a structure. This spectrum suggests that the AuNPs of the selected dimension supports formation of a sharp peak at about 568 nm. Interestingly, another peak at about 440 nm is also visible. Figure 6c shows the mode profile of the AuNP at the wavelength of 568 nm, indicating a significant field enhancement factor ( $P_{\rm enh}$ ) inside the 5 nm TMD layer. In fact, in the upper side of this layer  $P_{\text{enh}}$  is close to 15 and in the lower side  $P_{\rm enh}$  reduces to about 4. Note that the wavelength of this mode (568 nm) is close to the maximum peak responsivity of the photodetectors based on application of WS2-NDs on graphene.<sup>58</sup> This suggests the possibility of coupling of the plasmon modes of the WS2-NDs with those of the AuNPs, forming heterogeneous plasmonic dimmers. Such dimmers can offer more favorable field plasmon modes, particularly inside the 5 nm thick dielectric layer, leading to ultrahigh SERS sensitivities observed in this paper. 59,600

Figure 6d shows that mode profile of the AuNP at 532 nm wavelength that is the wavelength of the laser used to excite the samples was 532 nm (Figure 6b, square). While the  $P_{\rm enh}$  is smaller than that at the peak wavelength of the extinction spectrum, considerable enhancement remain as exhibited in Figure 6d. Specifically, the field enhancement factor  $P_{\rm enh}$  at the upper edge, middle and lower edge of the 5 nm thick TMD layer are respectively 10, 3, and 2. This suggests the laser intensity on the WS<sub>2</sub>–NDs can be significantly enhanced by the plasmonic effects of the AuNPs.

# 4. CONCLUSION

In summary, this work established a novel SERS substrate with extra high sensitivity-based plasmonic AuNP/WS2-ND/ graphene vdW heterostructures. This substrate integrates two plasmonic nanostructures of AuNPs and WS2-NDs, and the DFT and FDTD simulations indicate that the improved dipole dipole interaction together with charge transfer at the vdW interfaces plays a critical role to enable superposition of their LSPR effects. This has been confirmed experimentally in observations of enhanced graphene Raman signatures and enhanced SERS sensitivity of R6G probe molecules on the AuNP/WS<sub>2</sub>-ND/graphene vdW heterostructure, comparing to that on WS<sub>2</sub>-ND/graphene and AuNP/graphene substrates. Specifically, the graphene's G-peak intensity is enhanced by 7.8fold by the combination of AuNPs and WS2-NDs, in contrast to 5.3 or 4.0 folds respectively by WS2-NDs or AuNPs alone. Moreover, the high R6G SERS sensitivity of  $1 \times 10^{-12}$  M achieved on the AuNP/WS<sub>2</sub>-ND/graphene substrates is one or three orders of magnitude enhancement over that of on the WS<sub>2</sub>-ND/graphene or AuNP/graphene, respectively. Furthermore, this sensitivity is two to four orders of magnitude better than that on the TMDs/metal nanostructure SERS substrates

and at least an order of magnitude better than the best SERS substrates reported in previous works. This result therefore demonstrates a new pathway in superposition of the LSPR effect from two different kinds of plasmonic nanostructures via vdW heterostructures. Finally, the developed layer-by-layer synthesis process of transfer-free CVD growth of WS<sub>2</sub>–ND/graphene followed with in vacuo decoration of the AuNPs can be scale-up for run-to-run synthesis of the AuNP/WS<sub>2</sub>–ND/graphene vdW heterostructures SERS substrates for commercialization.

#### ASSOCIATED CONTENT

## **5** Supporting Information

The Supporting Information is available free of charge at https://pubs.acs.org/doi/10.1021/acsanm.9b02472.

SERS spectra and histogram and Raman spectra (PDF)

#### AUTHOR INFORMATION

#### **Corresponding Authors**

Samar Ali Ghopry — Department of Physics and Astronomy, University of Kansas, Lawrence, Kansas 66045, United States; o orcid.org/0000-0002-2135-8306; Email: s461g593@ ku.edu

Judy Z. Wu — Department of Physics and Astronomy, University of Kansas, Lawrence, Kansas 66045, United States; Email: jwu@ ku.edu

#### **Authors**

Mohammed Alamri — Department of Physics and Astronomy, University of Kansas, Lawrence, Kansas 66045, United States; orcid.org/0000-0002-7473-8644

**Ryan Goul** – Department of Physics and Astronomy, University of Kansas, Lawrence, Kansas 66045, United States

Brent Cook — Department of Physics and Astronomy, University of Kansas, Lawrence, Kansas 66045, United States;
orcid.org/0000-0001-9288-7267

Seyed M. Sadeghi — Department of Physics, The University of Alabama in Huntsville, Huntsville, Alabama 35899, United States

Rithvik R. Gutha — Department of Physics and Astronomy, Living Systems Institute, University of Exeter, Exeter EX4 4QD, United Kingdom

Ridwan Sakidja — Department of Physics, Astronomy, and Materials Science, Missouri State University, Springfield, Missouri 65897, United States

Complete contact information is available at: https://pubs.acs.org/10.1021/acsanm.9b02472

## **Author Contributions**

S.G and J.W. proposed the experiment. S.G., M.A., R.G., and B.G. provided the characterization of the samples. S.G. and M.A. contributed to sample fabrication. S.S., R.R., and R.S. worked on the simulation. S.G. and J.W. wrote the manuscript. All authors participated in the improvement of the manuscript.

#### Notes

The authors declare no competing financial interest.

## ACKNOWLEDGMENTS

The authors acknowledge support in part by U.S. Army Research Office Contract ARO-W911NF-16-1-0029 and National Science Foundation Contracts NSF-ECCS-1809293/1809284, NSF-DMR-1508494, and NSF-DMR-1909292. S.A.G. acknowledges the support from Jazan University.

#### REFERENCES

- (1) Fang, Y.; Seong, N. H.; Dlott, D. D. Measurement of the distribution of site enhancements in surface-enhanced Raman scattering. *Science* **2008**, *321* (5887), 388–92.
- (2) Lin, H. X.; Li, J. M.; Liu, B. J.; Liu, D. Y.; Liu, J.; Terfort, A.; Xie, Z. X.; Tian, Z. Q.; Ren, B. Uniform gold spherical particles for single-particle surface-enhanced Raman spectroscopy. *Phys. Chem. Chem. Phys.* **2013**, *15* (12), 4130–5.
- (3) Potara, M.; Baia, M.; Farcau, C.; Astilean, S. Chitosan-coated anisotropic silver nanoparticles as a SERS substrate for single-molecule detection. *Nanotechnology* **2012**, 23 (5), 055501.
- (4) Sivashanmugan, K.; Liao, J. D.; Liu, B. H.; Yao, C. K. Focused-ion-beam-fabricated Au nanorods coupled with Ag nanoparticles used as surface-enhanced Raman scattering-active substrate for analyzing trace melamine constituents in solution. *Anal. Chim. Acta* **2013**, *800*, 56–64.
- (5) Camden, J. P.; Dieringer, J. A.; Wang, Y.; Masiello, D. J.; Marks, L. D.; Schatz, G. C.; Van Duyne, R. P. Probing the structure of single-molecule surface-enhanced Raman scattering hot spots. *J. Am. Chem. Soc.* **2008**, *130* (38), 12616–7.
- (6) Dieringer, J. A.; Lettan, R. B., 2nd; Scheidt, K. A.; Van Duyne, R. P. A frequency domain existence proof of single-molecule surface-enhanced Raman spectroscopy. *J. Am. Chem. Soc.* **2007**, *129* (51), 16249–56.
- (7) Bell, S. E.; Sirimuthu, N. M. Surface-enhanced Raman spectroscopy (SERS) for sub-micromolar detection of DNA/RNA mononucleotides. *J. Am. Chem. Soc.* **2006**, *128* (49), 15580–1.
- (8) Cao, Y. C.; Jin, R.; Mirkin, C. A. Nanoparticles with Raman spectroscopic fingerprints for DNA and RNA detection. *Science* **2002**, 297 (5586), 1536–40.
- (9) Ling, X.; Moura, L. G.; Pimenta, M. A.; Zhang, J. Charge-Transfer Mechanism in Graphene-Enhanced Raman Scattering. *J. Phys. Chem. C* **2012**, *116* (47), 25112–25118.
- (10) Guerrini, L.; Graham, D. Molecularly-mediated assemblies of plasmonic nanoparticles for Surface-Enhanced Raman Spectroscopy applications. *Chem. Soc. Rev.* **2012**, *41* (21), 7085–107.
- (11) Mu, C.; Zhang, J. P.; Xu, D. Au nanoparticle arrays with tunable particle gaps by template-assisted electroless deposition for high performance surface-enhanced Raman scattering. *Nanotechnology* **2010**, *21* (1), 015604.
- (12) Tan, Y.; Ma, L.; Gao, Z.; Chen, M.; Chen, F. Two-Dimensional Heterostructure as a Platform for Surface-Enhanced Raman Scattering. *Nano Lett.* **2017**, *17* (4), 2621–2626.
- (13) Huh, S.; Park, J.; Kim, Y. S.; Kim, K. S.; Hong, B. H.; Nam, J. M. UV/ozone-oxidized large-scale graphene platform with large chemical enhancement in surface-enhanced Raman scattering. *ACS Nano* **2011**, 5 (12), 9799–806.
- (14) Ling, X.; Xie, L.; Fang, Y.; Xu, H.; Zhang, H.; Kong, J.; Dresselhaus, M. S.; Zhang, J.; Liu, Z. Can graphene be used as a substrate for Raman enhancement? *Nano Lett.* **2010**, *10* (2), 553–61.
- (15) Xie, L.; Ling, X.; Fang, Y.; Zhang, J.; Liu, Z. Graphene as a substrate to suppress fluorescence in resonance Raman spectroscopy. *J. Am. Chem. Soc.* **2009**, *131* (29), 9890–1.
- (16) Xu, W.; Mao, N.; Zhang, J. Graphene: a platform for surface-enhanced Raman spectroscopy. *Small* **2013**, 9 (8), 1206–24.
- (17) Ling, X.; Fang, W.; Lee, Y. H.; Araujo, P. T.; Zhang, X.; Rodriguez-Nieva, J. F.; Lin, Y.; Zhang, J.; Kong, J.; Dresselhaus, M. S. Raman enhancement effect on two-dimensional layered materials: graphene, h-BN and MoS2. *Nano Lett.* **2014**, *14* (6), 3033–40.
- (18) Novoselov, K. S.; Mishchenko, A.; Carvalho, A.; Castro Neto, A. H. 2D materials and van der Waals heterostructures. *Science* **2016**, *353* (6298), aac9439.
- (19) Qiu, H.; Li, Z.; Gao, S.; Chen, P.; Zhang, C.; Jiang, S.; Xu, S.; Yang, C.; Li, H. Large-area MoS2 thin layers directly synthesized on Pyramid-Si substrate for surface-enhanced Raman scattering. *RSC Adv.* **2015**, 5 (102), 83899–83905.
- (20) Xu, Y. Y.; Yang, C.; Jiang, S. Z.; Man, B. Y.; Liu, M.; Chen, C. S.; Zhang, C.; Sun, Z. C.; Qiu, H. W.; Li, H. S.; Feng, D. J.; Zhang, J. X. Layer-controlled large area MoS 2 layers grown on mica substrate for

- surface-enhanced Raman scattering. Appl. Surf. Sci. 2015, 357, 1708–1713
- (21) Yin, Y.; Miao, P.; Zhang, Y.; Han, J.; Zhang, X.; Gong, Y.; Gu, L.; Xu, C.; Yao, T.; Xu, P.; Wang, Y.; Song, B.; Jin, S. Significantly Increased Raman Enhancement on MoX2 (X = S, Se) Monolayers upon Phase Transition. *Adv. Funct. Mater.* **2017**, 27 (16), 1606694–1606702.
- (22) Zhang, Y.; Chang, T. R.; Zhou, B.; Cui, Y. T.; Yan, H.; Liu, Z.; Schmitt, F.; Lee, J.; Moore, R.; Chen, Y.; Lin, H.; Jeng, H. T.; Mo, S. K.; Hussain, Z.; Bansil, A.; Shen, Z. X. Direct observation of the transition from indirect to direct bandgap in atomically thin epitaxial MoSe2. *Nat. Nanotechnol.* **2014**, *9* (2), 111–5.
- (23) Kim, H.; Lee, D.-H.; Son, Y.-A. Electrochemical Study on Rhodamine 6G-Indole Based Dye for HOMO and LUMO Energy Levels. *Textile Coloration and Finishing* **2013**, 25 (1), 7–12.
- (24) Guthmuller, J.; Champagne, B. Resonance Raman Scattering of Rhodamine 6G as Calculated by Time-Dependent Density Functional Theory: Vibronic and Solvent Effects. *J. Phys. Chem. A* **2008**, *112*, 3215–3223.
- (25) Lee, Y.; Kim, H.; Lee, J.; Yu, S. H.; Hwang, E.; Lee, C.; Ahn, J. H.; Cho, J. H. Enhanced Raman Scattering of Rhodamine 6G Films on Two-Dimensional Transition Metal Dichalcogenides Correlated to Photoinduced Charge Transfer. *Chem. Mater.* **2016**, 28 (1), 180–187. (26) Bednorz, J. G.; Muller, K. A. Possible High-Tc Superconductivity
- (26) Bednorz, J. G.; Muller, K. A. Possible High-Tc Superconductivity in the Ba-La-Cu-O System. *Z. Phys. B: Condens. Matter* **1986**, *64* (2), 189–193.
- (27) Anbazhagan, R.; Vadivelmurugan, A.; Tsai, H.-C.; Jeng, R.-J. Surface-enhanced Raman scattering of alkyne-conjugated MoS2: a comparative study between metallic and semiconductor phases. *J. Mater. Chem. C* **2018**, *6* (5), 1071–1082.
- (28) Ghopry, S.; Alamri, M.; Goul, R.; Sakidja, R.; Wu, J. Extraordinary Sensitivity of Surface-Enhanced Raman Spectroscopy of Molecules on MoS2 (WS2) Nanodomes/Graphene van der Waals Heterostructure Substrates. *Adv. Opt. Mater.* **2019**, *7*, 1801249–1801259.
- (29) Gamucci, A.; Spirito, D.; Carrega, M.; Karmakar, B.; Lombardo, A.; Bruna, M.; Pfeiffer, L. N.; West, K. W.; Ferrari, A. C.; Polini, M.; Pellegrini, V. Anomalous low-temperature Coulomb drag in graphene-GaAs heterostructures. *Nat. Commun.* **2014**, *5*, 5824.
- (30) Georgiou, T.; Jalil, R.; Belle, B. D.; Britnell, L.; Gorbachev, R. V.; Morozov, S. V.; Kim, Y. J.; Gholinia, A.; Haigh, S. J.; Makarovsky, O.; Eaves, L.; Ponomarenko, L. A.; Geim, A. K.; Novoselov, K. S.; Mishchenko, A. Vertical field-effect transistor based on graphene-WS2 heterostructures for flexible and transparent electronics. *Nat. Nanotechnol.* **2013**, *8* (2), 100–3.
- (31) Levendorf, M. P.; Kim, C. J.; Brown, L.; Huang, P. Y.; Havener, R. W.; Muller, D. A.; Park, J. Graphene and boron nitride lateral heterostructures for atomically thin circuitry. *Nature* **2012**, *488* (7413), 627–32.
- (32) Lu, R.; Konzelmann, A.; Xu, F.; Gong, Y.; Liu, J.; Liu, Q.; Xin, M.; Hui, R.; Wu, J. Z. High sensitivity surface enhanced Raman spectroscopy of R6G on in situ fabricated Au nanoparticle/graphene plasmonic substrates. *Carbon* **2015**, *86*, 78–85.
- (33) Xu, W.; Ling, X.; Xiao, J.; Dresselhaus, M. S.; Kong, J.; Xu, H.; Liu, Z.; Zhang, J. Surface enhanced Raman spectroscopy on a flat graphene surface. *Proc. Natl. Acad. Sci. U. S. A.* **2012**, *109* (24), 9281–6.
- (34) Liu, Y.; Luo, F. Spatial Raman mapping investigation of SERS performance related to localized surface plasmons. *Nano Res.* **2020**, *13* (1), 138–144.
- (35) Liu, Y.; Luo, F. Large-scale highly ordered periodic Au nanodiscs/graphene and graphene/Au nanoholes plasmonic substrates for surface-enhanced Raman scattering. *Nano Res.* **2019**, *12* (11), 2788– 2795.
- (36) Goul, R.; Das, S.; Liu, Q.; Xin, M.; Lu, R.; Hui, R.; Wu, J. Z. Quantitative analysis of surface enhanced Raman spectroscopy of Rhodamine 6G using a composite graphene and plasmonic Au nanoparticle substrate. *Carbon* **2017**, *111*, 386–392.
- (37) Xu, G. W.; Liu, J. W.; Wang, Q.; Hui, R. Q.; Chen, Z. J.; Maroni, V. A.; Wu, J. Plasmonic Graphene Transparent Conductors. *Adv. Mater.* **2012**, 24 (10), OP71–OP76.

- (38) Xu, S.; Jiang, S.; Wang, J.; Wei, J.; Yue, W.; Ma, Y. Graphene isolated Au nanoparticle arrays with high reproducibility for high-performance surface-enhanced Raman scattering. *Sens. Actuators, B* **2016**, 222, 1175–1183.
- (39) Chen, P. X.; Qiu, H. W.; Xu, S. C.; Liu, X. Y.; Li, Z.; Hu, L. T.; Li, C. H.; Guo, J.; Jiang, S. Z.; Huo, Y. Y. A novel surface-enhanced Raman spectroscopy substrate based on a large area of MoS 2 and Ag nanoparticles hybrid system. *Appl. Surf. Sci.* **2016**, *375*, 207–214.
- (40) Shorie, M.; Kumar, V.; Kaur, H.; Singh, K.; Tomer, V. K.; Sabherwal, P. Plasmonic DNA hotspots made from tungsten disulfide nanosheets and gold nanoparticles for ultrasensitive aptamer-based SERS detection of myoglobin. *Microchim. Acta* **2018**, *185* (3), 158.
- (41) Alamri, M.; Sakidja, R.; Goul, R.; Ghopry, S.; Wu, J. Z. Plasmonic Au Nanoparticles on 2D MoS2/Graphene van der Waals Heterostructures for High-Sensitivity Surface-Enhanced Raman Spectroscopy. ACS Applied Nano Materials 2019, 2 (3), 1412–1420.
- (42) Cook, B.; Liu, Q.; Liu, J.; Gong, M.; Ewing, D.; Casper, M.; Stramel, A.; Wu, J. Facile zinc oxide nanowire growth on graphene via a hydrothermal floating method: towards Debye length radius nanowires for ultraviolet photodetection. *J. Mater. Chem. C* **2017**, *5* (38), 10087–10092
- (43) Gong, M.; Liu, Q.; Cook, B.; Kattel, B.; Wang, T.; Chan, W. L.; Ewing, D.; Casper, M.; Stramel, A.; Wu, J. Z. All-Printable ZnO Quantum Dots/Graphene van der Waals Heterostructures for Ultrasensitive Detection of Ultraviolet Light. ACS Nano 2017, 11 (4), 4114–4123.
- (44) Xu, G.; Liu, J.; Wang, Q.; Hui, R.; Chen, Z.; Maroni, V. A.; Wu, J. Plasmonic Graphene Transparent Conductors. *Adv. Mater.* **2012**, 24 (10), OP71–OP76.
- (45) Kohn, W.; Sham, L. J. Self-Consistent Equations Including Exchange and Correlation Effects. *Phys. Rev.* **1965**, *140* (4A), A1133–A1138.
- (46) Kresse, G.; Furthmuller, J. Efficient iterative schemes for ab initio total-energy calculations using a plane-wave basis set. *Phys. Rev. B: Condens. Matter Mater. Phys.* **1996**, 54 (16), 11169–11186.
- (47) Chen, C. T.; Pedrini, J.; Gaulding, E. A.; Kastl, C.; Calafiore, G.; Dhuey, S.; Kuykendall, T. R.; Cabrini, S.; Toma, F. M.; Aloni, S.; Schwartzberg, A. M. Very High Refractive Index Transition Metal Dichalcogenide Photonic Conformal Coatings by Conversion of ALD Metal Oxides. *Sci. Rep.* **2019**, *9* (1), 2768.
- (48) Li, Y. L.; Chernikov, A.; Zhang, X.; Rigosi, A.; Hill, H. M.; van der Zande, A. M.; Chenet, D. A.; Shih, E. M.; Hone, J.; Heinz, T. F. Measurement of the optical dielectric function of monolayer transitionmetal dichalcogenides: MoS2, MoSe2, WS2, and WSe2. *Phys. Rev. B: Condens. Matter Mater. Phys.* **2014**, 90 (20), 205422.
- (49) Liu, H. L.; Shen, C. C.; Su, S. H.; Hsu, C. L.; Li, M. Y.; Li, L. J. Optical properties of monolayer transition metal dichalcogenides probed by spectroscopic ellipsometry. *Appl. Phys. Lett.* **2014**, *105* (20), 201905.
- (50) Mahigir, A.; Chang, T. W.; Behnam, A.; Liu, G. L.; Gartia, M. R.; Veronis, G. Plasmonic nanohole array for enhancing the SERS signal of a single layer of graphene in water. *Sci. Rep.* **2017**, *7* (1), 14044.
- (51) Zhang, S. G.; Zhang, X. W.; Liu, X.; Yin, Z. G.; Wang, H. L.; Gao, H. L.; Zhao, Y. J. Raman peak enhancement and shift of few-layer graphene induced by plasmonic coupling with silver nanoparticles. *Appl. Phys. Lett.* **2014**, *104* (12), 121109–121114.
- (52) Zhao, W.; Ghorannevis, Z.; Amara, K. K.; Pang, J. R.; Toh, M.; Zhang, X.; Kloc, C.; Tan, P. H.; Eda, G. Lattice dynamics in mono- and few-layer sheets of WS2 and WSe2. *Nanoscale* **2013**, *5* (20), 9677–83.
- (53) Huh, S.; Park, J.; Kim, Y. S.; Kim, K. S.; Hong, B. H.; Nam, J.-M. UV/ozone-oxidized large-scale graphene platform with large chemical enhancement in surface-enhanced Raman scattering. *ACS Nano* **2011**, 5 (12), 9799–9806.
- (54) Hou, M.-J.; Zhang, X.; Cui, X.-Y.; Liu, C.; Li, Z.-C.; Zhang, Z.-J. Preparation of SiO2@ Au nanorod array as novel surface enhanced Raman substrate for trace pollutants detection. *Chin. Phys. B* **2015**, 24 (3), 034203.
- (55) Lu, Z.; Si, H.; Li, Z.; Yu, J.; Liu, Y.; Feng, D.; Zhang, C.; Yang, W.; Man, B.; Jiang, S. Sensitive, reproducible, and stable 3D plasmonic

- hybrids with bilayer WS2 as nanospacer for SERS analysis. *Opt. Express* **2018**, 26 (17), 21626–21641.
- (56) Li, M.; Zhang, J.; Suri, S.; Sooter, L. J.; Ma, D.; Wu, N. Detection of adenosine triphosphate with an aptamer biosensor based on surface-enhanced Raman scattering. *Anal. Chem.* **2012**, *84* (6), 2837–42.
- (57) Shi, Y.; Wang, H.; Jiang, X.; Sun, B.; Song, B.; Su, Y.; He, Y. Ultrasensitive, Specific, Recyclable, and Reproducible Detection of Lead Ions in Real Systems through a Polyadenine-Assisted, Surface-Enhanced Raman Scattering Silicon Chip. *Anal. Chem.* **2016**, *88* (7), 3723–9.
- (58) Alamri, M.; Gong, M.; Cook, B.; Goul, R.; Wu, J. Z. Plasmonic WS2 Nanodiscs/Graphene van der Waals Heterostructure Photodetectors. ACS Appl. Mater. Interfaces 2019, 11 (36), 33390–33398.
- (59) Oubre, C.; Nordlander, P. Finite-difference time-domain studies of the optical properties of nanoshell dimers. *J. Phys. Chem. B* **2005**, *109* (20), 10042–10051.
- (60) Romero, I.; Aizpurua, J.; Bryant, G. W.; Garcia De Abajo, F. J. Plasmons in nearly touching metallic nanoparticles: singular response in the limit of touching dimers. *Opt. Express* **2006**, *14* (21), 9988–9999.